

STABILIZED INVARIANT ENERGY QUADRATIZATION (S-IEQ) METHOD FOR THE MOLECULAR BEAM EPITAXIAL MODEL WITHOUT SLOPE SECTION

HUI ZHANG, XIAOFENG YANG, AND JUN ZHANG

Abstract. The design of numerical approaches for the molecular beam epitaxy models has always been a hot issue in numerical analysis, in which one of the main challenges for algorithm design is how to establish a high-order time-accurate numerical method with unconditional energy stability. The numerical method developed in this paper is based on the “stabilized-Invariant Energy Quadratization” (S-IEQ) approach. Its novelty is that by adding a very simple linear stabilization term, the difficulty that the original energy potential for the no-slope selection case is not bounded from below can be easily overcome. Then by using the standard format of the IEQ method, we can easily obtain a linear, unconditionally energy stable, and second-order time accurate scheme for solving the system. We further implement various numerical examples to demonstrate the stability and accuracy of the proposed scheme.

Key words. Molecular beam epitaxy, linear, second-order, unconditional energy stability.

1. Introduction

Molecular Beam Epitaxy (MBE) model refers to a continuum model to describe the growth of crystalline layer deposited on a substrate. By using a scalar variable to represent the height of the crystalline layer, the model is derived by using the gradient flow approach in L^2 space. The postulated energy of the system is composed of a linear entropy and a nonlinear potential where the nonlinear potential can take two forms, one is the fourth-order Ginzburg-Landau double-well potential and the model built on that is called the slope selection model, and the other is the logarithmic potential and the model built on it is called the no-slope selection model. Since the algorithm development for the double-well potential of the slope selection model has been extensively studied, see [11, 15, 17, 20, 21, 30], in this paper, we consider the numerical approximations of the no-slope selection model, i.e., the time marching scheme for the logarithmic potential. Formally, the governing system of the MBE model with no-slope selection is not complicated where only two terms (a linear term and a nonlinear term) are involved. However, it is still very challenging to develop an effective numerical scheme due to the complexity of the logarithmic format of the nonlinear term.

Here, we briefly introduce the available numerical schemes for the MBE no-slope selection model here. According to the discretization method of the nonlinear potential, the available approaches can be categorized to the following two types, explicit type and semi-implicit type. The explicit type methods includes the operator splitting approach [10], explicit method [11], stabilized-explicit method [8, 13], convex-splitting method [17], and ETD approaches [3–5, 9], etc. The semi-implicit approach includes the quadratization approach, including the Invariant Energy Quadratization (IEQ) method [30] and its various version of Scalar Auxiliary Variable (SAV) method [7], etc. It is worth noting that almost all available schemes are linear and their implementation are very effective practically (e.g., most schemes

only need to solve linear systems with variable coefficients or even constant coefficients at each time step). Among so many effective algorithms that can be used to solve the MBE model, considering that the process of constructing and implementing the quadratization type scheme is relatively simpler and easier, in this article we use IEQ method to solve the model.

However, the choice of the IEQ method raises a direct open question. Although the IEQ method developed in [30] enables one to construct linear, second-order, and unconditionally energy stable schemes for a large class of gradient flows, it is problematic whether it is applicable for solving the MBE model without slope selection since the nonlinear logarithmic potential is not obviously bounded from below. To overcome it, in this paper, we modify the IEQ approach to the stabilized version where we modify the total free energy by adding a gradient potential. With the help of it, we can easily show that the boundedness (from below) can be naturally satisfied, and the second-order time marching scheme can be obtained easily. Note that the total free energy of the model has not changed, because while adding that gradient term, we also subtract it and the subtracted item can be further bounded by the higher-order linear potential. In this way, the bounded-from-below property of the total free energy can still be strictly guaranteed. Moreover, the magnitude of the stabilization term can be arbitrarily small as long as it is positive, which implies that the splitting error caused by this term can actually be controlled within the machine precision. We further prove the well-posedness of the developed scheme and also show that the constructed scheme is unconditionally energy stable.

The structure of this article is as follows. In Section 2, the MBE model without slope selection is briefly introduced. The numerical scheme is further constructed in Section 3. The practical implementation process is also given in detail. The unconditional energy stability is proved rigorously. In Section 4, we implement the numerical simulations numerically to demonstrate the stability, accuracy of the developed schemes. In Section 5, we give some concluding remarks.

2. MBE model with no slope selection

We first give a brief introduction on the MBE model with no slope selection. The computed domain is set as $\Omega = [0, L]^d, d = 2$. Suppose $\phi(\mathbf{x})$ is a height function and the total phenomenological free energy is postulated as [11]

$$(1) \quad E(\phi) = \int_{\Omega} \left(L(\Delta\phi) + F(\nabla\phi) \right) d\mathbf{x},$$

where the $L(\Delta\phi) = \frac{\epsilon^2}{2}(\Delta\phi)^2$ is the linear entropy that represents the surface diffusion effect, the coefficient ϵ is used to controls the diffusive strength, and $F(\phi)$ is the nonlinear potential that represents a continuum description of the Ehrlich-Schwoebel effect. For the no slope selection case, $F(\nabla\phi)$ reads as

$$(2) \quad F(\nabla\phi) = -\frac{1}{2} \ln(1 + |\nabla\phi|^2).$$

The evolution equation for the height function ϕ is derived by using the gradient flow approach in the L^2 space, that reads as

$$(3) \quad \phi_t = -M(\epsilon^2 \Delta^2 \phi + f(\nabla\phi)),$$

where M is the mobility constant, and

$$(4) \quad f(\nabla\phi) = \nabla \cdot \left(\frac{\nabla\phi}{1 + |\nabla\phi|^2} \right).$$

The boundary conditions will be the periodic boundary condition or the no-flux boundary condition $\partial_{\mathbf{n}}\phi|_{\partial\Omega} = \partial_{\mathbf{n}}\Delta\phi|_{\partial\Omega} = 0$, where \mathbf{n} is the outward normal on the domain boundary $\partial\Omega$:

One can easily obtain the energy dissipation property for the model (3) mentioned above. We denote by $(f, g) = (\int_{\Omega} f(\mathbf{x})g(\mathbf{x})d\mathbf{x})^{\frac{1}{2}}$ the L^2 inner product between functions $f(\mathbf{x})$ and $g(\mathbf{x})$, by $\|f\| = (f, f)$ the L^2 norm of a function $f(\mathbf{x})$. By taking the L^2 inner product of (3) with ϕ_t and performing integration by parts, we obtain

$$(5) \quad \frac{d}{dt}E(\phi) = -\frac{1}{M}\|\phi_t\|^2 \leq 0.$$

By taking the L^2 inner product with 1 for (3), we obtain the mass conservation property as

$$(6) \quad \frac{d}{dt} \int_{\Omega} \phi d\mathbf{x} = 0.$$

Without loss of generality, the zero integral condition $\int_{\Omega} \phi(\mathbf{x})d\mathbf{x} = 0$ is assumed so that the Poincaré inequality holds, i.e., there exists a positive constant c_0 such that

$$(7) \quad \|\phi\| \leq c_0\|\nabla\phi\| \quad \forall \phi \in \bar{H}^1(\Omega) := \{\phi \in H^1(\Omega) : \int_{\Omega} \phi(\mathbf{x})d\mathbf{x} = 0\}.$$

3. Numerical scheme

We aim to develop a second-order time accurate, linear, and unconditionally energy stable scheme based on the IEQ approach. However, one will quickly discover that the nonlinear potential $F(\nabla\phi)$ is not bounded from below, so we cannot directly quadratize it. We need to find out how to establish the bounded-from-below property of the nonlinear potential. For this reason, we reformulate the total free energy to be the following equivalent form

$$(8) \quad E(\phi) = \int_{\Omega} \left(\frac{\epsilon^2}{2}(\Delta\phi)^2 - \frac{\eta}{2}|\nabla\phi|^2 \right) d\mathbf{x} + \int_{\Omega} \left(\frac{\eta}{2}|\nabla\phi|^2 + F(\nabla\phi) \right) d\mathbf{x},$$

where η is any positive constant.

Inspired from [7, 20], we establish a bounded-from-below property for the nonlinear and linear parts of the total free energy as follows.

Lemma 3.1. *For any $\eta > 0$, there holds the following inequality*

$$(9) \quad \frac{\eta}{2}|\nabla\phi|^2 - \frac{1}{2}\ln(1 + |\nabla\phi|^2) \geq C_B,$$

$$(10) \quad \int_{\Omega} \left(\frac{\epsilon^2}{2}(\Delta\phi)^2 - \frac{\eta}{2}|\nabla\phi|^2 \right) d\mathbf{x} > 0,$$

where $C_B = \frac{1}{2}(\ln\eta - \eta + 1)$.

Proof. For any $\eta > 0$, it is easy to show that the function $G(t) := \frac{\eta}{2}t - \frac{1}{2}\ln(1 + t)$ is always convex ($G''(t) > 0$). Hence we can find when $t^* = \frac{1}{\eta} - 1$, $G(t^*)$ reaches its minimum, i.e.,

$$(11) \quad \frac{\eta}{2}t - \frac{1}{2}\ln(1 + t) = G(t) \geq G(t^*) = \frac{1}{2}(\ln\eta - \eta + 1).$$

Then set $t = |\mathbf{y}|^2$, we obtain

$$(12) \quad \frac{1}{2}\eta|\mathbf{y}|^2 - \frac{1}{2}\ln(1 + |\mathbf{y}|^2) \geq \frac{1}{2}(\ln\eta - \eta + 1).$$

Let $\mathbf{y} = \nabla\phi$, we have

$$(13) \quad \frac{1}{2}\eta|\nabla\phi|^2 - \frac{1}{2}\ln(1 + |\nabla\phi|^2) \geq \frac{1}{2}(\ln\eta - \eta + 1),$$

that concludes (9).

From the Poincaré inequality, we derive

$$(14) \quad \|\nabla\phi\|^2 = -(\phi, \Delta\phi) \leq \|\phi\|\|\Delta\phi\| \leq c_0\|\nabla\phi\|\|\Delta\phi\| \leq \frac{1}{2}\|\nabla\phi\|^2 + \frac{c_0^2}{2}\|\Delta\phi\|^2.$$

That is to say, the following inequality holds,

$$(15) \quad \int_{\Omega} \frac{\eta}{2}|\nabla\phi|^2 d\mathbf{x} \leq \frac{\eta}{2}c_0^2 \int_{\Omega} |\Delta\phi|^2 d\mathbf{x}.$$

Thus, as long as we choose $\eta < \frac{\epsilon^2}{c_0^2}$, we have

$$(16) \quad \int_{\Omega} \left(\frac{\epsilon^2}{2}(\Delta\phi)^2 - \frac{\eta}{2}|\nabla\phi|^2 \right) d\mathbf{x} > 0,$$

that concludes (10). □

From (9), we are able to introduce an auxiliary variable $V(t)$ as

$$(17) \quad V(t) = \sqrt{\frac{\eta}{2}|\nabla\phi|^2 + F(\nabla\phi) + B},$$

where B is any constant such that $B + C_B > 0$. Hence, using ϕ and V , the total energy (8) becomes

$$(18) \quad E(\phi, V) = \int_{\Omega} \left(\frac{\epsilon^2}{2}(\Delta\phi)^2 - \frac{\eta}{2}|\nabla\phi|^2 + V^2 \right) d\mathbf{x} - B|\Omega|.$$

Correspondingly, we rewrite the PDE system (3) for as follows,

$$(19) \quad \phi_t + M(\epsilon^2\Delta^2\phi + \eta\Delta\phi + HV) = 0,$$

$$(20) \quad V_t = \frac{1}{2}H\phi_t,$$

where

$$(21) \quad H(\phi) = \frac{-\eta\Delta\phi + \nabla \cdot \left(\frac{\nabla\phi}{1+|\nabla\phi|^2} \right)}{\sqrt{\frac{\eta}{2}|\nabla\phi|^2 + F(\nabla\phi) + B}}.$$

Note that the boundary conditions of the new system (19)-(20) are the same as the original system since the equation for V is just an ODE for time. The initial conditions for the system read as

$$(22) \quad \phi|_{t=0} = \phi^0, \quad V|_{t=0} = V(\phi^0).$$

The transformed PDE systems (19)-(20) still admits the energy dissipative laws. In details, by taking the L^2 inner product of (19) with ϕ_t and of (20) with V , then performing integration by parts and summing up both equalities, we obtain

$$(23) \quad \frac{d}{dt}E(\phi, V) = -\frac{1}{M}\|\phi_t\|^2 \leq 0.$$

We are now ready to construct the expected scheme based on the IEQ approach [22–32]. For simplicity, we consider only the time marching scheme. The stability results carry over to any version fully discretized schemes using Galerkin approaches without any further difficulties. Let $\delta t > 0$ be a time step size and set $t^n = n\delta t$ for $0 \leq n \leq N = [T/\delta t]$, let ψ^n denotes the numerical approximation to $\psi(\cdot, t)|_{t=t^n}$, and $\psi^* = 2\psi^n - \psi^{n-1}$ for any function ψ .

Assuming that ϕ^{n-1} , ϕ^n and V^{n-1} , V^n are known, we solve ϕ^{n+1} and V^{n+1} based on the second-order backward differentiation formula as follows,

$$(24) \quad \frac{a\phi^{n+1} - b\phi^n + c\phi^{n-1}}{2M\delta t} + \epsilon^2\Delta^2\phi^{n+1} + \eta\Delta\phi^{n+1} + H^*V^{n+1} = 0,$$

$$(25) \quad aV^{n+1} - bV^n + cV^{n-1} = \frac{1}{2}H^*(a\phi^{n+1} - b\phi^n + c\phi^{n-1}),$$

where $a = 3, b = 4, c = 1, H^* = H(\phi^*)$ with $\phi^* = 2\phi^n - \phi^{n-1}$. Note that as long as we set $a = 2, b = 2, c = 0$, the algorithm becomes first-order time accurate which can be applied to get ϕ^1 and V^1 .

We show that the scheme (24)-(25) is unconditionally energy stable as below.

Theorem 3.1. *The scheme (24)-(25) is unconditionally energy stable in the sense that it satisfies the following discrete energy dissipation law:*

$$(26) \quad \frac{1}{\delta t}(E^{n+1} - E^n) \leq -\frac{1}{M} \left\| \frac{3\phi^{n+1} - 4\phi^n + \phi^{n-1}}{2\delta t} \right\|^2,$$

where E^{n+1} is defined as:

$$(27) \quad \begin{aligned} E^{n+1} = & \frac{\epsilon^2}{4} (\|\Delta\phi^{n+1}\|^2 + \|\Delta(2\phi^{n+1} - \phi^n)\|^2) \\ & - \frac{\eta}{4} (\|\nabla\phi^{n+1}\|^2 + \|\nabla(2\phi^{n+1} - \phi^n)\|^2) \\ & + \frac{1}{2} (\|V^{n+1}\|^2 + \|2V^{n+1} - V^n\|^2) - B|\Omega|, \end{aligned}$$

and $E^{n+1} \geq -B|\Omega|$ is uniformly bounded from below.

Proof. By taking the inner product of (24) with $\frac{1}{2}(3\phi^{n+1} - 4\phi^n + \phi^{n-1})$ in L^2 , and applying the following identity

$$(28) \quad \begin{aligned} 2(3u - 4v + w, u) = & (|u|^2 + |2u - v|^2) - (|v|^2 + |2v - w|^2) \\ & + |u - 2v + w|^2, \end{aligned}$$

we obtain

$$(29) \quad \begin{aligned} & \frac{1}{4M\delta t} \|3\phi^{n+1} - 4\phi^n + \phi^{n-1}\|^2 + \frac{\epsilon^2}{4} (\|\Delta\phi^{n+1}\|^2 + \|2\Delta\phi^{n+1} - \Delta\phi^n\|^2) \\ & - \frac{\epsilon^2}{4} (\|\Delta\phi^n\|^2 + \|2\Delta\phi^n - \Delta\phi^{n-1}\|^2) + \frac{\epsilon^2}{4} \|\Delta\phi^{n+1} - 2\Delta\phi^n + \Delta\phi^{n-1}\|^2 \\ & - \frac{\eta}{4} (\|\nabla\phi^{n+1}\|^2 + \|2\nabla\phi^{n+1} - \Delta\phi^n\|^2) \\ & + \frac{\eta}{4} (\|\nabla\phi^n\|^2 + \|2\nabla\phi^n - \nabla\phi^{n-1}\|^2) - \frac{\eta}{4} \|\nabla\phi^{n+1} - 2\nabla\phi^n + \nabla\phi^{n-1}\|^2 \\ & + \frac{1}{2} (H^*V^{n+1}, (3\phi^{n+1} - 4\phi^n + \phi^{n-1})) = 0. \end{aligned}$$

By taking the L^2 inner product of (25) with V^{n+1} , we find

$$(30) \quad \begin{aligned} & \frac{1}{2} (\|V^{n+1}\|^2 + \|2V^{n+1} - V^n\|^2) - \frac{1}{2} (\|V^n\|^2 + \|2V^n - V^{n-1}\|^2) \\ & + \frac{1}{2} \|V^{n+1} - 2V^n + V^{n-1}\|^2 \\ & = \frac{1}{2} (V^{n+1}H^*, (3\phi^{n+1} - 4\phi^n + \phi^{n-1})). \end{aligned}$$

Combining (29) and (30) and using Lemma 3.1, we arrive at

$$\begin{aligned}
 & \frac{\epsilon^2}{4} (\|\Delta\phi^{n+1}\|^2 + \|2\Delta\phi^{n+1} - \Delta\phi^n\|^2) \\
 & - \frac{\epsilon^2}{4} (\|\Delta\phi^n\|^2 + \|2\Delta\phi^n - \Delta\phi^{n-1}\|^2) \\
 & - \frac{\eta}{4} (\|\nabla\phi^{n+1}\|^2 + \|2\nabla\phi^{n+1} - \Delta\phi^n\|^2) \\
 (31) \quad & + \frac{\eta}{4} (\|\nabla\phi^n\|^2 + \|2\nabla\phi^n - \nabla\phi^{n-1}\|^2) \\
 & + \frac{1}{2} (\|V^{n+1}\|^2 + \|2V^{n+1} - V^n\|^2) - \frac{1}{2} (\|V^n\|^2 + \|2V^n - V^{n-1}\|^2) \\
 & + \left\{ \frac{\epsilon^2}{4} \|\Delta\phi^{n+1} - 2\Delta\phi^n + \Delta\phi^{n-1}\|^2 - \frac{\eta}{4} \|\nabla\phi^{n+1} - 2\nabla\phi^n + \nabla\phi^{n-1}\|^2 \right. \\
 & \left. + \frac{1}{2} \|V^{n+1} - 2V^n + V^{n-1}\|^2 \right\} = -\frac{\delta t}{M} \left\| \frac{3\phi^{n+1} - 4\phi^n + \phi^{n-1}}{2\delta t} \right\|^2.
 \end{aligned}$$

From (10), it is easy to see that the terms in $\{\}$ are positive. By dropping the terms in $\{\}$, we obtain the desired result (26). Moreover, from (10), it is easy to see that E^{n+1} is uniformly bounded from below as $E^{n+1} \geq -B|\Omega|$. \square

We further show how to solve the constructed scheme (24)-(25) in practice. Instead of solving the coupled system between ϕ^{n+1} and V^{n+1} , we reformulate (25) to the following:

$$(32) \quad V^{n+1} = \frac{1}{2} H^* \phi^{n+1} + g^n,$$

where $g^n = \frac{1}{3}(4V^n - V^{n-1}) - \frac{1}{6}H^*(4\phi^n - \phi^{n-1})$. By replacing V^{n+1} in (24) with (32), it is easy to find that ϕ^{n+1} is the solution of the following linear system

$$(33) \quad A\phi = b,$$

where

$$(34) \quad \begin{cases} A\phi = \frac{3}{2M\delta t}\phi + \epsilon^2\Delta^2\phi + \eta\Delta\phi + \frac{1}{2}H^*H^*\phi, \\ b = \frac{4\phi^n - \phi^{n-1}}{2\delta t} - H^*g^n. \end{cases}$$

To solve (33), we consider its weak form. Namely, find $\phi \in H^2(\Omega)$, such that

$$\begin{aligned}
 (35) \quad & \left(\frac{3}{2M\delta t}\phi, \psi \right) + \epsilon^2(\Delta\phi, \Delta\psi) - \eta(\nabla\phi, \nabla\psi) \\
 & + \frac{1}{2}(H^*\phi, H^*\psi) = (b, \psi), \forall \psi \in H^2(\Omega).
 \end{aligned}$$

It is easy to show that the bilinear system (35) is well-posed by using the Lax-Milgram Theorem (coercivity and boundedness are obvious), i.e., there exists the unique solution. Meanwhile, Note that the linear system (35) is symmetric positive definite, therefore we can apply many well-known fast solvers like CG or PCG to solve it efficiently.

Remark 3.1. *The key to constructing the IEQ scheme for the MBE no-slope selection model is to establishing the bounded-from-below property for the energy potential. Without it, the definition of the new variable U and the law of energy dissipation (26) are meaningless, since the radicand maybe negative, and the energy E^{n+1} may tend to $-\infty$. The term $\frac{\eta}{2}|\nabla\phi|^2$ works as the stabilization term indeed. Moreover, note that Lemma (3.1) is valid for any arbitrarily small η , which*

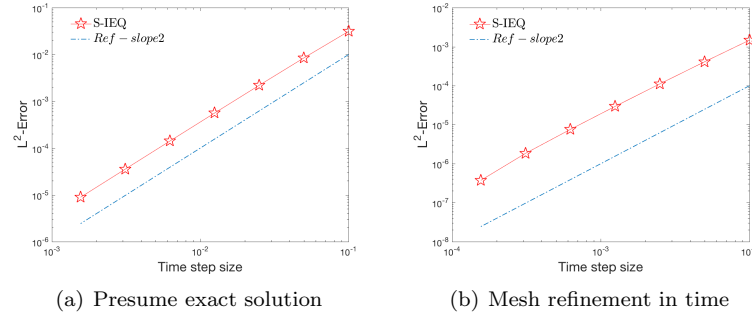


FIGURE 1. Convergence order tests for (a) the example of the presumed exact solutions (36); and (b) the time step refinement example with initial conditions given in (37).

means that the splitting error caused by this stabilization term can be arbitrarily small. Moreover, based on the same method to handle the total free energy, one can establish another version of quadratization approach, SAV method, to construct a similar second-order time marching scheme.

Similar stabilization techniques had been widely used in the numerical scheme for solving the nonlinear models with high stiffness, e.g., the methods of linear stabilization, IEQ, SAV, convex-splitting methods, etc., see [1, 2, 6, 18, 19, 22, 28, 29, 31, 32].

Remark 3.2. For the system (19)-(20), another alternative second-order scheme of Crank-Nicolson type can be constructed in the similar way, and we leave it the interested readers. Although we only carry out the semi-discrete time marching scheme, the fully-discrete version can be further developed without any essential difficulties.

4. Numerical simulations

In this section, we verify the stability/accuracy of the proposed scheme (24)-(25), and perform some benchmark simulations to show its effectiveness. The computational domain is set as a rectangular 2D domain with $(x, y) \in \Omega = [0, L]^2$. We adopt the Fourier-spectral method to discretize the space.

4.1. Accuracy tests. We first perform several convergence tests to verify the accuracy and stability of the finite element scheme (24)-(25), referred to as S-IEQ for short.

We impose some source term to the system (3) such that the exact solutions read as:

$$(36) \quad \phi(x, y, t) = \sin(x)\cos(y)\cos t,$$

Assuming that the domain is $\Omega = [0, 2\pi]^2$ and the periodic boundary conditions are satisfied, we set the order parameters as $\epsilon^2 = 0.1$, $M = 1$, $\eta = 1e-10$, $B = 100$.

To verify the temporal convergence order, we discretize the space using 256 Fourier modes so that the grid size is sufficiently small and the spatial discretization errors are negligible compared with the time discretization error. In Fig. 1 (a), the L^2 -errors between the numerical solution and the exact solution at $t = 1$ are plotted, where we vary different time step size δt . It can be observed that the scheme S-IEQ presents perfect second-order convergence rate.

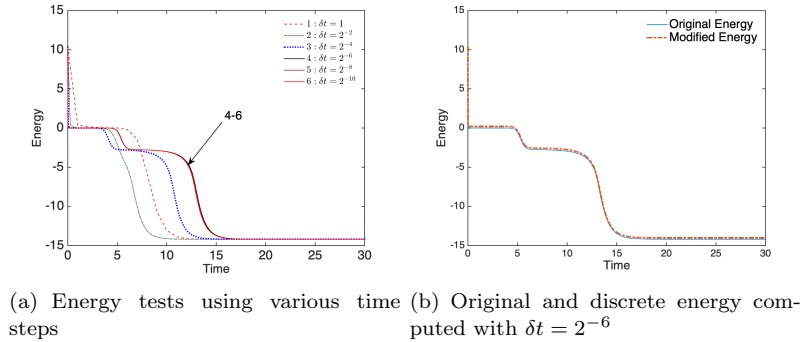


FIGURE 2. (a) The comparisons of the time evolution of the total free energy (27) computed by using various time steps; and (b) the comparison of the original free energy (1) and the discrete energy (27) computed by using the time step $\delta t = 2^{-6}$.

Furthermore, without pre-assigning the exact solution, we set the initial condition ϕ^0 and compute the accuracy order by using different time step size δt . The computational region is still set as the 2D computational domain of $\Omega = [0, 2\pi]^2$, and the initial conditions are set as

$$(37) \quad \phi^0 = \sin(2x)\cos(3y).$$

We still discretize the space using 256 Fourier modes, and refine the time step size δt . Since the exact solutions are not known for this example, we assume that the numerical solution computed with $\delta t = 1e-6$ is treated as the exact solution to obtain computation errors. The model parameters are still set as the previous example. In Fig. 1 (b), the L^2 errors between the numerical solution and the exact solution at $t = 1$ are plotted, where different time step sizes δt are used. The convergence order illustrated by the test also display the perfect second-order time accuracy.

4.2. Energy Stability tests. We further implement a numerical example to testify whether the energy stability of the scheme S-IEQ can be maintained as expected. The example is a benchmark numerical test given in [11, 12, 16, 20, 30]. where the initial conditions are set as

$$(38) \quad \phi(x, y, 0) = 0.1(\sin(3x)\sin(2y) + \sin(5x)\sin(5y)).$$

The computational domain is set as $[0, 2\pi]^2$ and 256^2 Fourier modes are used to discretize the space. The model parameters are set as $\epsilon^2 = 0.1$, $M = 1$, $\eta = 1e-10$, $B = 100$.

We test the energy stability of the scheme S-IEQ by using various time steps. In Fig. 2 (a), the evolution curves of the total free energy (27) computed by the scheme S-IEQ are plotted, in which all obtained energy curves show monotonic decays, thereby verifying its unconditional energy stability. Moreover, when the time step is sufficiently small (e.g. $\delta t \leq 2^{-6}$), the obtained energy curves completely overlap, indicating that the smaller the time step, the more accurate the obtained solution is. When the time step is larger (e.g. $\delta t \geq 2^{-4}$), the obtained energy curves deviate significantly from those accurate energy curves computed using smaller time steps, indicating that the time step is larger, the error is also large although the scheme is stable. In Fig. 2 (b), the evolution curve of the original energy (1) and the modified

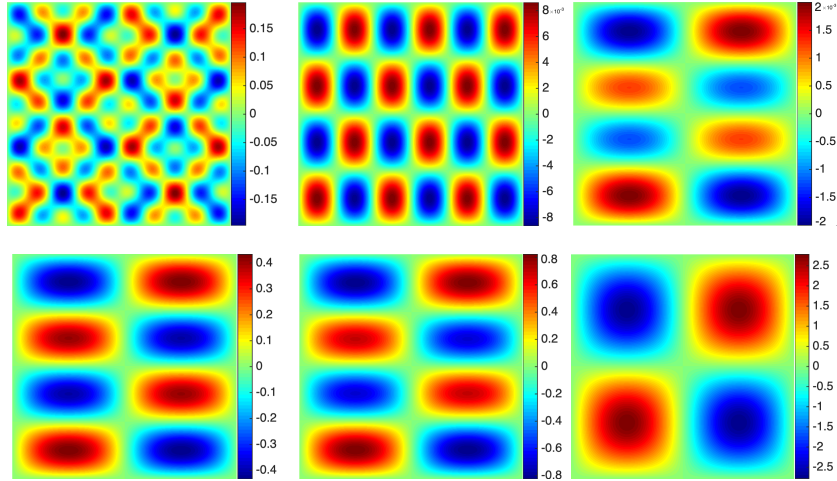


FIGURE 3. Snapshots of the profile ϕ taken at $t = 0, 0.6, 2.4, 4.8, 8,$ and 30 .

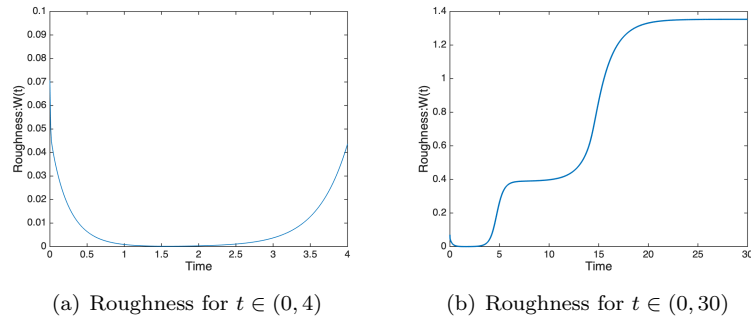


FIGURE 4. The time evolution of the roughness function $W(t)$ computed using $\delta t = 2^{-6}$.

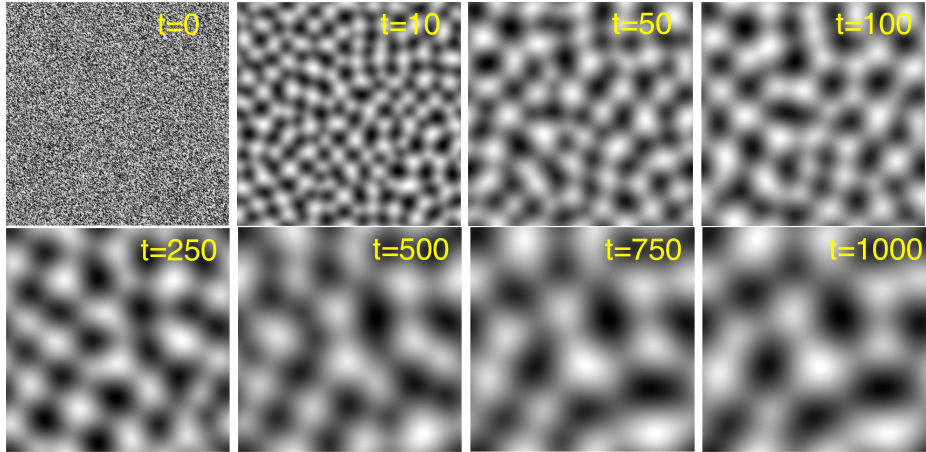
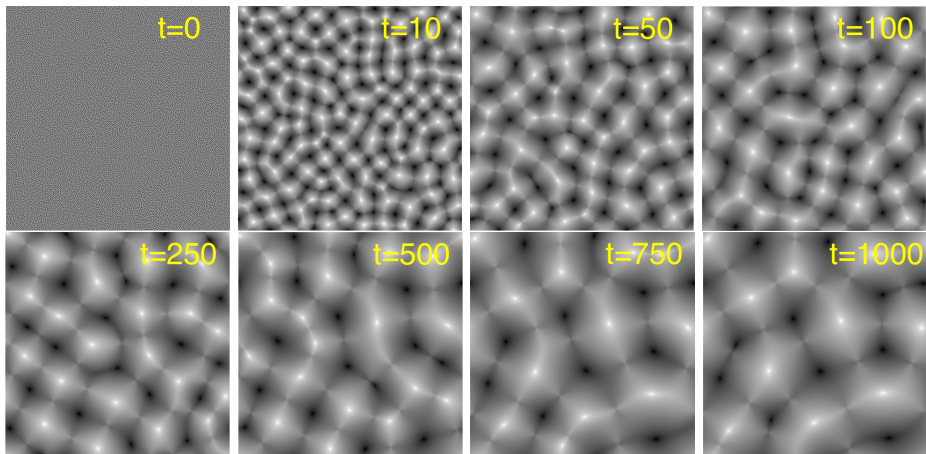
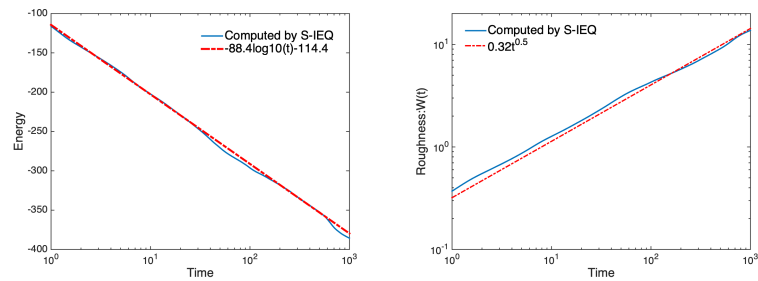
discrete energy (27) computed by using $\delta t = 2^{-6}$ are plotted, and we find that the two energy evolution curves completely overlap, without any visible difference.

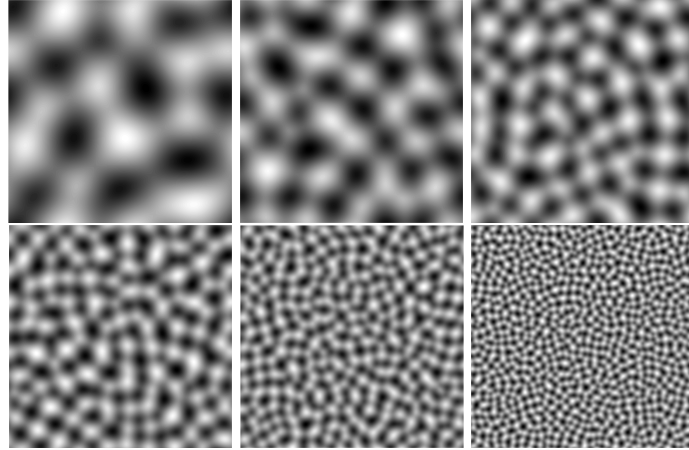
In Fig. 3, snapshots of the profiles of ϕ at different times are plotted until the steady-state. In Fig. 4, using $\delta t = 2^{-6}$, we plot the time evolution of the so-called “roughness” measure function that is a good quantity to evaluate the deviation of the height function, defined as (cf. [11, 20, 30]):

$$(39) \quad W(t) = \sqrt{\frac{1}{|\Omega|} \int_{\Omega} (\phi(\mathbf{x}, t) - \bar{\phi}(t))^2 d\mathbf{x}},$$

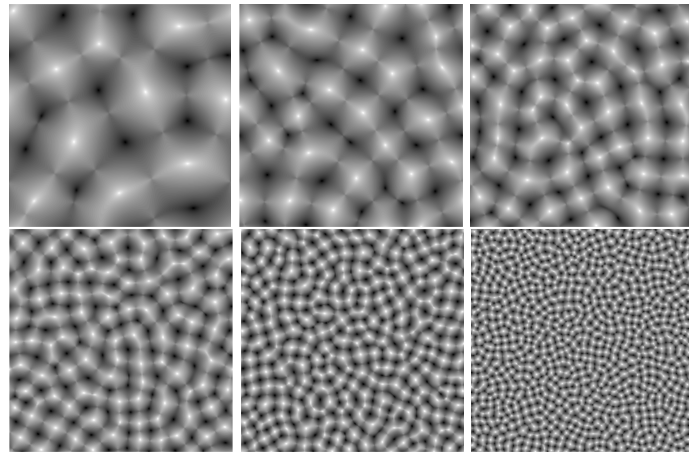
where $\bar{\phi}(t) = \frac{1}{|\Omega|} \int_{\Omega} \phi(\mathbf{x}, t) d\mathbf{x}$. The time evolution curve of $W(t)$ shown in Fig. 4 displays that the deviation decreases for a short period and then keep increasing until the steady-state.

4.3. Coarsening dynamics. We implement another benchmark problems of the MBE model (cf. [3, 4, 7–9, 11, 13, 15, 17, 20, 21, 30]), the so-called coarsening dynamics to verify the effectiveness of the proposed scheme S-IEQ, The initial conditions are set as the random number ranging from -0.001 to 0.001 , and the model parameters

(a) Snapshots of ϕ at different times(b) Snapshots of $\Delta\phi$ at different timesFIGURE 5. Snapshots of the profile ϕ and $\Delta\phi$ taken at different times (time t is shown in each subfigure).(a) Semi-log of energy evolution over (b) Log-log of roughness $W(t)$ over time timeFIGURE 6. The time evolution of (a) the total free energy (27) (semi-log over time), and (b) the roughness function $W(t)$ (log-log over time) computed using $\delta t = 1e-3$.



(a) Profiles of ϕ with $\epsilon = 0.03, 0.01, 0.005, 0.0025, 0.001, 0.0005$ (from left to right and from top to bottom)



(b) Profiles of $\Delta\phi$ with $\epsilon = 0.03, 0.01, 0.005, 0.0025, 0.001, 0.0005$ (from left to right and from top to bottom)

FIGURE 7. Snapshots of the profile ϕ and $\Delta\phi$ taken at steady-state ($t = 1000$) with various ϵ .

are set as

$$(40) \quad \epsilon = 0.03, M = 1, \eta = 1e-10, B = 100.$$

The computational domain is set as $\Omega = [0, 4\pi]^2$ which is discretized by using 256^2 Fourier modes. We set the time step $\delta t = 1e-3$ for better accuracy.

In Fig. 5, we show snapshots of the height function ϕ and its Laplacian $\Delta\phi$ calculated at different times. We observe the growth of the thin films, and the pyramid/anti-pyramid shapes of hills and valleys form over time. In Fig. 6 (a) and (b), we plot the time evolution of the total free energy (27) (semi-log over time) and the roughness function $W(t)$ (log-log over time), respectively. We observe that the energy decays at the rate of $-\log_{10}(t)$, while the roughness increases at the rate $t^{0.5}$. In Fig. 7, we compare the steady-state solutions of ϕ and $\Delta\phi$ with various diffusive coefficient ϵ , where we find that smaller ϵ causes the density of

pyramid/anti-pyramid of hills and valleys greater. By comparing the numerical results given in [7, 12, 14, 16, 20, 30], we find that the calculation results of the S-IEQ scheme are consistent with them quantitatively, thus verifying the computational effectiveness of the developed scheme.

5. Concluding remarks

In this paper, we solve the problem that the MBE model with no slope selection can be handled by the IEQ type approach even if the nonlinear part of the energy potential is not obviously bounded from below. After adding the stabilization term with an artificially small magnitude, we prove that the bounded-from-below property still holds for the modified nonlinear potential. Then a linear and second-order time accurate BDF2 scheme is established, which brings up the so-called stabilized-IEQ scheme. We only need to solve a symmetric positive definite system at each time step. The unconditional energy stability is rigorously proved, and various numerical simulations are implemented to verify the effectiveness of the developed scheme, numerically.

Acknowledgments

The work of Xiaofeng Yang was partially supported by National Science Foundation with grant numbers DMS-1818783 and DMS-2012490. The work of Jun Zhang was supported by the National Natural Science Foundation of China (Nos. 12026241, 12026240, 11901132 and 62062018), Guizhou Key Laboratory of Big Data Statistics Analysis (No. BDSA20200102) and Natural Science Research Projects of Education Department of Guizhou Province (KY [2021]015).

References

- [1] C. Chen and X. Yang. Efficient numerical scheme for a dendritic solidification phase field model with melt convection. *J. Comput. Phys.*, 388:41–62, 2019.
- [2] C. Chen and X. Yang. Fast, provably unconditionally energy stable, and second-order accurate algorithms for the anisotropic Cahn-Hilliard Model. *Comput. Meth. Appl. Mech. Engrg.*, 351:35–59, 2019.
- [3] W. Chen, W. Li, Z. Luo, C. Wang, and X. Wang. A stabilized second order exponential time differencing multistep method for thin film growth model without slope selection. *Mathematical Modeling and Numerical Analysis*, 54:727–750, 2020.
- [4] W. Chen, W. Li, C. Wang, S. Wang, and X. Wang. Energy stable higher order linear etd multi-step methods for gradient flows: application to thin film epitaxy. *Research in the Mathematical Sciences*, 7:13, 2020.
- [5] K. Cheng, Z. Qiao, and C. Wang. A third order exponential time differencing numerical scheme for no-slope-selection epitaxial thin film model with energy stability. *Journal of Scientific Computing*, 81:154–185, 2019.
- [6] K. Cheng, C. Wang, and S. M. Wise. An Energy Stable BDF2 Fourier Pseudo-Spectral Numerical Scheme for the Square Phase Field Crystal Equation. *Comm in Comput. Phys.*, 26:1335–1364, 2019.
- [7] Q. Cheng, J. Shen, and X. Yang. Highly efficient and accurate numerical schemes for the epitaxial thin film growth models by using the SAV approach. *J. Sci. Comput.*, 78:1467–1487, 2019.
- [8] Y. Hao, Q. Huang, and C. Wang. A third order bdf energy stable linear scheme for the no-slope-selection thin film model. in press, *Communications in Computational Physics*, 2020.
- [9] L. Ju, X. Li, Z. Qiao, and H. Zhang. Energy stability and error estimates of exponential time differencing schemes for the epitaxial growth model without slope selection. *Mathematics of Computation*, 87:1859–1885, 2017.
- [10] H. G. Lee, J. Shin, and JY. Lee. A second-order operator splitting fourier spectral method for models of epitaxial thin film growth. *J. Sci. Comput.*, 71:13031318, 2017.
- [11] B. Li and J.-G. Liu. Thin film epitaxy with or without slope selection. *European J. Appl. Math.*, 14:713–743, 2003.

- [12] B. Li and J. G. Liu. Epitaxial growth without slope selection: energetics, coarsening, and dynamic scaling. *J. Non. Sci.*, 14(5):429–451, 2004.
- [13] W. Li, W. Chen, C. Wang, Y. Yan, and R. He. A second order energy stable linear scheme for a thin film model without slope selection. *Journal of Scientific Computing*, 76:1905–1937, 2018.
- [14] D. Moldovan and L. Golubovic. Interfacial coarsening dynamics in epitaxial growth with slope selection. *Physical Review E*, 61(6):6190, 2000.
- [15] Z. Qiao, Z. Sun, and Z. Zhang. The stability and convergence of two linearized finite difference schemes for the nonlinear epitaxial growth model. *Num. Meth. Par. Diff. Eqns*, 28(6):1893–1915, 2012.
- [16] Z. Qiao, Z. Zhang, and T. Tang. An adaptive time-stepping strategy for the molecular beam epitaxy models. *SIAM. J. Sci. Comput.*, 33(3):1395–1414, 2011.
- [17] J. Shen, C. Wang, S. Wang, and X. Wang. Second-order convex splitting schemes for gradient flows with ehrlich-schwoebel type energy: application to thin film epitaxy. *SIAM. J. Numer. Anal.*, 50:105–125, 2012.
- [18] J. Shen and X. Yang. Numerical approximations of Allen–Cahn and Cahn–Hilliard equations. *Disc. Cont. Dyn. Sys. A*, 28:1669–1691, 2010.
- [19] J. Shen and X. Yang. The IEQ and SAV approaches and their extensions for a class of highly nonlinear gradient flow systems. *Contemporary Mathematics*, 754:217–245, 2020.
- [20] C. Wang, X. Wang, and S. M. Wise. Unconditionally stable schemes for equations of thin film epitaxy. *Discrete Contin. Dyn. Syst.*, 28(1):405–423, 2010.
- [21] C. Xu and T. Tang. Stability analysis of large time-stepping methods for epitaxial growth models. *SIAM J. Num. Anal.*, 44:1759–1779, 2006.
- [22] X. Yang. Linear, first and second order and unconditionally energy stable numerical schemes for the phase field model of homopolymer blends. *J. Comput. Phys.*, 327:294–316, 2016.
- [23] X. Yang. A new efficient Fully-decoupled and Second-order time-accurate scheme for Cahn-Hilliard phase-field model of three-phase incompressible flow. *Computer Methods in Applied Mechanics and Engineering*, 376:13589, 2021.
- [24] X. Yang. A novel fully-decoupled scheme with second-order time accuracy and unconditional energy stability for the Navier-Stokes equations coupled with mass-conserved Allen-Cahn phase-field model of two-phase incompressible flow. *International Journal for Numerical Methods in Engineering*, 122:1283–1306, 2021.
- [25] X. Yang. A novel fully-decoupled, second-order and energy stable numerical scheme of the conserved Allen-Cahn type flow-coupled binary surfactant model. *Computer Methods in Applied Mechanics and Engineering*, 373:113502, 2021.
- [26] X. Yang. A novel fully-decoupled, second-order time-accurate, unconditionally energy stable scheme for a flow-coupled volume-conserved phase-field elastic bending energy model. *Journal of Computational Physics*, 432:110015, 2021.
- [27] X. Yang. Numerical approximations of the Navier-Stokes equation coupled with volume-conserved multi-phase-field vesicles system: fully-decoupled, linear, unconditionally energy stable and second-order time-accurate numerical scheme. *Computer Methods in Applied Mechanics and Engineering*, 375:113600, 2021.
- [28] X. Yang and H. Yu. Efficient Second Order Unconditionally Stable Schemes for a Phase Field Moving Contact Line Model Using an Invariant Energy Quadraticization Approach. *SIAM J. Sci. Comput.*, 40:B889–B914, 2018.
- [29] X. Yang and G.-D. Zhang. Convergence Analysis for the Invariant Energy Quadraticization (IEQ) Schemes for Solving the Cahn-Hilliard and Allen-Cahn Equations with General Non-linear Potential. *Journal of Scientific Computing*, 82:55, 2020.
- [30] X. Yang, J. Zhao, and Q. Wang. Numerical approximations for the molecular beam epitaxial growth model based on the invariant energy quadraticization method. *J. Comput. Phys.*, 333:104–127, 2017.
- [31] X. Yang, J. Zhao, Q. Wang, and J. Shen. Numerical Approximations for a three components Cahn-Hilliard phase-field Model based on the Invariant Energy Quadraticization method. *M3AS: Mathematical Models and Methods in Applied Sciences*, 27:1993–2030, 2017.
- [32] J. Zhang and X. Yang. Unconditionally energy stable large time stepping method for the L2-gradient flow based ternary phase-field model with precise nonlocal volume conservation. *Computer Methods in Applied Mechanics and Engineering*, 361:112743, 2020.

School of Mathematical Sciences, Guizhou Normal University, Guiyang, 550025, China
E-mail: zhanghui@gznu.edu.cn

Department of Mathematics, University of South Carolina, Columbia, SC 29208, USA.
E-mail: xfyang@math.sc.edu

Corresponding author. Guizhou Key Laboratory of Big Data Statistics Analysis; Computational Mathematics Research Center, Guizhou University of Finance and Economics, Guiyang, 550025, China
E-mail: jzhang@mail.gufe.edu.cn